Conformational Changes in SP-B as a Function of Surface Pressure

Wilfred K. Fullagar,* Karen A. Aberdeen,* David G. Bucknall,† Paulus A. Kroon,* and Ian R. Gentle*
*School of Molecular and Microbial Sciences, The University of Queensland, Brisbane, Queensland 4072, Australia; and
†Department of Materials, University of Oxford, Oxford OX1 3PH, United Kingdom

ABSTRACT X-ray reflectivity of bovine and sheep surfactant-associated protein B (SP-B) monolayers is used in conjunction with pressure-area isotherms and protein models to suggest that the protein undergoes changes in its tertiary structure at the air/water interface under the influence of surface pressure, indicating the likely importance of such changes to the phenomena of protein squeeze out as well as lipid exchange between the air-water interface and subphase structures. We describe an algorithm based on the well-established box- or layer-models that greatly assists the fitting of such unknown scattering-length density profiles, and which takes the available instrumental resolution into account. Scattering-length density profiles from neutron reflectivity of bovine SP-B monolayers on aqueous subphases are shown to be consistent with the exchange of a large number of labile protons as well as the inclusion of a significant amount of water, which is partly squeezed out of the protein monolayer at elevated surface pressures.

INTRODUCTION

The fluid lining the interface of the alveoli, known as natural lung surfactant (NLS), has been the subject of intense research during the last decade, leading to major reviews in recent years (Review Issue of Biochimica et Biophysica Acta, 1998; Review Issue of Comparative Biochemistry and Physiology, 2001; Review Issue of Pediatric Pathology and Molecular Medicine, 2001). Components in this fluid are recognized as critical to various aspects of lung function, the most obvious of which is the need to preserve a very low surface tension at the air-fluid interface. A low surface tension prevents pulmonary collapse such as is associated with respiratory distress syndrome (RDS), and which is a common cause of death in premature infants. The primary surfactant associated with this low surface tension is the zwitterionic lipid dipalmitoylphosphatidylcholine (DPPC), though anionic lipids, in particular dipalmitoylphosphatidylglycerol (DPPG) are also known to have an important role (Oviedo et al., 2001; Takamoto et al., 2001). By themselves, these lipids do not have the transport properties required in order to accommodate changes in the area of the alveolus during the breathing cycle, and three of the four surfactant-associated proteins (SP-A, SP-B, and SP-C) have been implicated as having roles in these processes (Casals, 2001; Haagsman and Diemel, 2001).

The most enigmatic of the surfactant proteins is SP-B, which forms the subject of this work. It is the only surfactant protein critical to lung function, as shown by animal studies, and is a disulfide-linked homodimer, each half consisting of 79 amino acids. An excellent review of its known properties is given by Weaver (Weaver and Conkright, 2001). It has a strong overall positive charge at physiological pH. A structural model has been presented by Zaltash which is based on similarities with NK-lysin (Zaltash et al., 2000), a simplified version of which was presented earlier by Cruz (Cruz et al., 1995). Essentially, in the model of Zaltash, the protein consists of five amphipathic α-helices, folded such that the protein's hydrophobic faces are buried. The relative positioning of the helices is largely constrained by three internal disulfide bonds within each monomer. Given its critical role in normal lung function, and highly conserved primary structure, it is probable that SP-B's modus operandi does not vary from one species to the next. In what follows we provide evidence to suggest that SP-B unfolds to present its hydrophobic interior when present as a monolayer at the interface, and propose that this conformational change plays an important part of its normal duty cycle in the presence of lipids.

MATERIALS AND PROCEDURES

The experiments described here involved sheep and cow SP-B obtained on a number of different occasions using an adaptation (Perez-Gil et al., 1993) of the method of Curstedt (Curstedt et al., 1987). Fluid from lavaged or minced lungs was centrifuged at 20,000 $\times$ g for 30 min before extracting the pellet into chloroform/methanol according to the procedure originally described by Bligh and Dyer (Bligh and Dyer, 1959). The lower (organic) phase was evaporated to a few milliliters, applied to an 80 $\times$ 2 cm column of Sephadex LH-20 and eluted using a 2:1 $CHCl_3$:methanol (v/v) solvent mixture while monitoring the absorbance at 280 nm. The first peak from this column contained the hydrophobic proteins, which were pooled, dried under N_2, and immediately redissolved in ~5 mL of 1:1 $CHCl_3$:methanol + 5% 0.1 M $HCl_{(aq)}$. This was applied to a 60 $\times$ 2 cm Sephadex LH-60 size-exclusion chromatography column and eluted using the latter solvent system under ~2 m head of pressure. This second column effected a separation of SP-B, SP-C, and

Submitted January 13, 2003, and accepted for publication June 17, 2003.
Address reprint requests to Dr. Ian Gentle, School of Molecular and Microbial Sciences, The University of Queensland, Brisbane, Queensland 4072, Australia. Tel.: +61-7-3365-4800; Fax: +61-7-3365-4299; E-mail: i.gentle@uq.edu.au.

0006-3495/03/10/2624/09 $2.00

remaining lipid components comparable to that observed by Pérez-Gil (Pérez-Gil et al., 1993). Analysis of the putative SP-B fractions by SDS-PAGE (14% tris-tricine) stained using Coomassie blue showed a major protein band corresponding to an apparent molecular mass in the range of 20–30 kDa. Under reducing conditions (β-mercaptoethanol) the apparent molecular mass reduced to 5–6 kDa. Peptide sequencing was performed on the Western blot transfer of one such gel, which confirmed that SP-B was present, in addition to contaminants including α- and β-hemoglobin. Electrospray mass spectral analysis indicated that sheep and cow SP-B exist as dimers with molecular masses of 17,430 Da (sheep) and 17,450 Da (cow). The latter result is consistent with that of Nag (Nag et al., 1999).

Bovine SP-B was used in neutron reflectivity measurements, whereas for the x-ray reflectivity measurements SP-B from both sheep and cows was used. The subphase used was either 0.15 M NaCl containing 0.01 M HEPES (unadjusted pH ~5.5), or 0.10 M NaCl containing 0.01 M HEPES, (pH 7.2). Neutron scattering gives the opportunity to vary the subphase contrast by partial or complete deuteration of the water, and subphases of D_2O, 50% H_2O:D_2O mixtures (elsewhere referred to as HDO), and air contrast-matched water (elsewhere referred to as ACMW, composition $H_{1.842}D_{0.158}O$) were used. Calculation of titration curves indicated that for a pH change from 5.5 to 7.2 the charge of the dimeric protein would change from +11.5 to +10.1 in either species. (Database and facilities are available via http://au.expasy.org/.) It therefore seems unlikely that the modest differences in salinity or pH would lead to significant differences in the interfacial behavior of SP-B. Films were spread directly from LH-60 eluent solutions, and all measurements were done at 22.5°C.

Reflectometry measurements were carried out on Teflon Langmuir troughs (NIMA Technologies, Coventry, UK) using the angle-dispersive x-ray reflectometer (Schlossman et al., 1997) at beamline X-19C of the National Synchrotron Light Source, NY, USA, (λ = 1.54 Å), and neutron measurements were performed on the energy-dispersive CRISP reflectometer (Penfold et al., 1987) at the ISIS spallation source at Rutherford Appleton Laboratory, Didcot, UK (angle of incidence = 1.5°). Surface pressure-area measurements complement each reflectivity profile. Because the angle-dispersive x-ray reflectivity curves cover many orders of magnitude in intensity, and to compensate for changes in the x-ray beam footprint at the interface as a function of angle, these data were collected in (typically) nine regions of momentum transfer $Q = (4\pi/\lambda)\sin\theta$. An appropriate combination of input slit width, measurement time, and brass attenuators in front of the detector was used for each region. These data regions were made to overlap slightly in order to permit their subsequent rescaling. Analysis of the reflectivity curves was performed using the programs Parratt32 (Hahn Meitner Institute), SURFace (see http://www.isis.rl.ac.uk/largescale/SURF/technical/surface.htm) or Wincxmulf (Wincxmulf is a version of software developed at ISIS and adapted for multiple constrained refinements (Wincxmulf_1) by A.S. Brown (Research School of Chemistry, Australian National University)), which are based on optical matrix formalisms (Brown et al., 1997; Penfold and Thomas, 1990). Although each has particular strengths and weaknesses, results are invariably comparable, so that the choice of program is essentially dictated by convenience.

RESULTS AND ANALYSIS

Isotherms

A number of isotherms of SP-B have been reported in the literature (Bunger et al., 2001; Krol et al., 2000; Oosterlaken-Dijksterhuis et al., 1991; Taneva and Keough, 1994; Taneva et al., 1998), and when plotted on the same scale they show a very considerable variation in limiting area (from ~20–120 nm^2 per dimer). Large variations exist even for material originating from the same species. This almost certainly arises from difficulties in establishing the concentration of the spread chloroform/methanol SP-B solutions. Taneva and Keough have carefully addressed the difficulty of obtaining accurate protein concentrations and therefore limiting areas in studies of porcine SP-B (Taneva and Keough, 1994). Since SP-B from different species has very similar primary structure (and therefore presumably higher structure also), we have opted to treat the concentration of our protein solutions as a variable parameter, which can be adjusted so that our SP-B isotherms agree with the isotherm published by Taneva under almost identical conditions. Examples of sheep and cow SP-B isotherms that have been fitted in this way are shown in Fig. 1.

An important aspect of the literature isotherms in which there does appear to be general consensus is the appearance of a plateau at $\Pi \sim$ 30–40 mN m^{-1}. This plateau, which occurs at ~15 nm^2 $molecule^{-1}$ in the illustrated isotherms, coincides with the first appearance during compression of faint visible streaks in the monolayer parallel to the advancing barrier and within a few centimeters of it. This observation demonstrates that the plateau corresponds to collapse of the protein monolayer which subsequently remains associated with the surface, an argument supported by the relatively small loss of material on subsequent slow cycles in Fig. 1. It also argues against attempting to interpret reflectometry results at smaller areas, as the surface will contain features on a length scale at least comparable to the wavelength of visible light. At such small areas the film loses its fluidity, so that the Wilhelmy plate is pushed in the direction of the barrier movement and will give a false reading. This is the likely explanation for apparent changes in the surface pressure at the smallest areas shown in Fig. 1. Further experiments (data not shown) demonstrate that the collapse pressure is independent of temperature over the range 15°C–45°C.

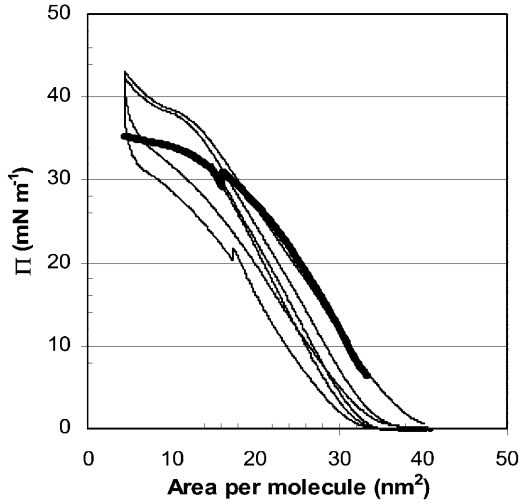

FIGURE 1 Heavy line is the compression isotherm for a bovine SP-B monolayer on 0.1M NaCl, 0.01M HEPES, pH 7.2 at 22.5°C. The discontinuity at ~16 nm^2 $molecule^{-1}$ corresponds to a point at which x-ray reflectivity data was measured, a process which took ~2 h. The light lines show the cycling behavior of a sheep SP-B monolayer under similar conditions. Closed (*open*) symbols represent compressions (expansions) of the film, these being done in the order ■, ▲, respectively. The entire sequence required a little over an hour. The relative lack of hysteresis in the third cycle (●, ○), which stops shy of the collapse at ~38 mN m^{-1}, demonstrates that the hysteresis is largely associated with changes that occur during collapse. During the second decompression (△), the barrier was stopped for a few minutes at ~18 nm^2 $molecule^{-1}$, the discontinuity in that curve further demonstrating the nonequilibrium nature of these isotherms. For both species the area per molecule has been scaled as described in the text.

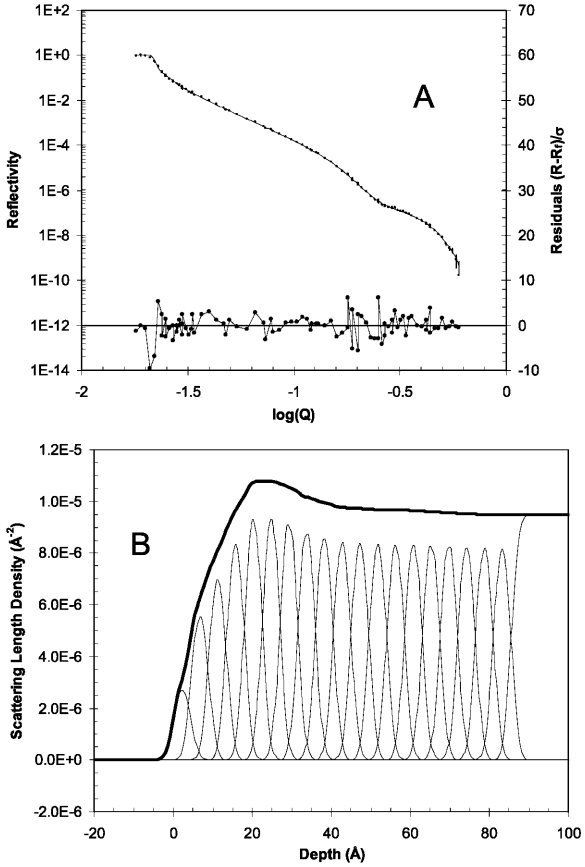

FIGURE 2 An example of x-ray reflectivity data showing error bars, fit, and residuals corresponding to sheep SP-B on saline buffer (0.1 M NaCl, 0.01 M HEPES, pH 7.2, 22°C) at 30 mN m^{-1} is shown in *A*. This was fitted using the DDP method described in the text, with the corresponding SLD profile shown in *B*. For this particular profile the densities of the 19 illustrated layers were simultaneously refined, the final (*bold*) line being the sum of the contributions from all the layers.

X-ray reflectivity

An example of an x-ray reflectivity profile and the corresponding fitted scattering-length density (SLD) profile is shown in Fig. 2. The x-ray models were generated by the following procedure, which we refer to as the discrete density profile (DDP) method. The procedure is equally applicable to neutron data, however these were modeled using the conventional box-models as described later. A model is established consisting of zero, one, two, or more layers, each with the same thickness t, and with roughness parameters σ constant throughout. We fix $\sigma \approx 1/Q_{max}$, and $t \approx 3\sigma$, where Q_{max} is the maximum momentum transfer at which coherent scattering is observable in the data set in question. For neutrons this would be the point at which the observed reflectivity has dropped to the level of the incoherent background scatter, whereas for x-rays it is rather more subjective, with error bars typically obscuring details for $Q > \sim 0.6$ $Å^{-1}$. The SLD of each layer is initially set to that of the subphase (ie. a reasonable starting estimate which introduces no steps except at the air interface where the most distinct step is anticipated) and then only the SLDs of the layers are refined. In this way the best model is the one that satisfactorily models the data using the least number of layers and is amenable to chemical interpretation. In practice we find it is almost invariably possible to quickly produce an excellent and chemically meaningful fit to our reflectivity data in this way; in related work we find that it readily reproduces the anticipated SLD profiles for phospholipids at interfaces, which are more commonly found by two-layer models in which thicknesses, roughnesses, and SLDs are all refined.

The rationale behind the DDP approach is as follows. The spatial resolution available in the data is determined by $d_{min} \approx \pi/Q_{max}$, where d_{min} is the minimum distance over which the data can resolve SLD gradients. These gradients are characterized in most reflectivity fitting packages by convolution of step functions with Gaussians of standard deviation σ (the roughness parameter). By fixing all such roughnesses in a model such that $3\sigma \approx d_{min}$, we ensure that we will not refine profile features sharper than the available data can resolve. Given that $3\sigma \approx d_{min} \approx \pi/Q_{max}$, the assignment $\sigma \approx 1/Q_{max}$ is reasonable. Consider digitizing an arbitrary SLD profile into a number of slabs of thickness t,

each with edges characterized by the parameter σ. In this way, a large number of very thin slabs would lead to a large number of parameters needing simultaneous refinement; moreover if the slabs were very thin they would be entirely smeared out after convolution with the Gaussian. On the other hand, very thick slabs will not permit digitization of an arbitrary SLD profile. The choice $t \approx 3\sigma$ represents a suitable compromise.

The approach proves very useful for systems involving monolayers whose total anticipated thickness is only several times greater than the calculated value of t. For thicker systems the number of layer SLDs requiring simultaneous refinement becomes unmanageable, with a corresponding growth in the number of local minima. In this situation one can do preliminary refinements using suitably thick and smeared layers to reduce the number of initially fitted densities and obtain a gross impression of the structure, then subdivide them and reduce the roughnesses until the instrumental resolution is obtained. This approach was not necessary in the profile models presented here, but has been shown to work nevertheless. Such models sometimes find their way into a local minimum; we find that this can often be addressed by temporarily changing the weighting scheme (Parratt32) or fitting algorithm (Wincxmulf) used to fit the data, though this was not necessary in any of the fits presented here. Fits presented here always minimize residuals calculated using the error bars obtained in the experiment.

The SLD profile found in this way can often be satisfactorily represented using a smaller number of layers of fitted thickness, SLD, and roughness in a way that requires fewer parameters and agrees with chemical intuition. In this context, situations commonly arise in which something is known about the system that can help pin down one or more parameters. For example, monolayer roughnesses at the air interface are unlikely to greatly exceed $\sigma \sim 3$ Å in phospholipid systems at high pressure, and synchrotron x-ray data confirms this (Helm et al., 1991). In fitting phospholipid neutron reflectivity data, in which the resolution is much poorer, the use of such a low value is otherwise very difficult to justify. Although permissible under such circumstances, we have not yet encountered a reflectivity profile in which it is impossible to produce a comparably good fit by direct application of the DDP method. Moreover, there are situations in which a symmetrically rough edge as refined by traditional layer approaches is inappropriate. The air-protein and protein-subphase interfaces observed in the x-ray SLD profiles in this work are examples of this, in which the DDP method permits a considerably more flexible and presumably realistic assessment of the form of the electron density gradient.

The fitted x-ray SLD profiles of ovine and bovine SP-B monolayers are generally comparable at similar surface pressures (see Fig. 4), consisting of a density maximum that broadens and moves to a greater depth as collapse of the film is approached. This strengthens our belief that bovine SP-B, though possibly structurally different from sheep and other sequenced mammals, essentially operates by the same mechanism.

Neutron reflectivity

Part of the difficulty in modeling the available neutron data lies in their relatively low information content, some consequences of which have been examined by Schalke (Schalke and Losche, 2000). In many individual cases satisfactory fits can be obtained by simply fitting an air-water roughness, or by allowing the air SLD to decay exponentially to the subphase SLD (available in Parratt32) with the only fitted parameter being the decay length. Synchrotron x-ray data, with its relatively small error bars and extended Q-range, necessitates much more critical fitting. Unfortunately the DDP method cannot be fruitfully used in simultaneous fits of the x-ray and neutron data because the thicknesses are not fitted. Turning to more traditional box methods, it must be remembered that the protein's x-ray SLD profile (which will have a significant contribution from the protein's sulfur atoms) is in all likelihood rather different from its neutron SLD profile (for which we anticipate a more uniform distribution, with a higher potential for proton/deuteron exchange in the hydrophilic parts of the molecule), so that without a strong impression of the structure and orientation of the protein, it is unclear how to mutually constrain the resulting layers. Simultaneous reflectivity fits based on evolution of molecular models (Politsch, 2001) are probably the long-term answer to this dilemma.

In the meantime, an appropriate compromise is to model the x-ray and neutron data independently. X-ray data was fitted using the DDP method, then models of the neutron data were fitted in which layer thicknesses were mutually constrained, with edge roughnesses fixed at the smallest value sensibly inferred from x-ray fits. Fig. 3 shows an example of such a neutron fit, in which the neutron roughnesses have been fixed at 3.0 Å (a value comparable to capillary waves in such systems (Braslau et al., 1988; Daillant et al., 1990; Schalke et al., 2000; Schalke and Losche, 2000)). In Fig. 4 the SLD profiles obtained in this way are compiled to permit meaningful comparison, whereas Table 1 lists the corresponding fitted neutron parameters.

From the fitted neutron parameters it is possible to estimate the amount of included water in the layers. An outline of this calculation follows. The amino acid sequence of the protein is known to a good approximation, and so also the number of potentially exchangeable protons n_l (we count $n_l = \sim 260$ per bovine dimer); it can be assumed that the mole fraction of D_2O in the subphase (χ_D) determines the extent of this exchange, which is essentially at equilibrium within ~15 min (Pastrana-Rios et al., 1995). We can estimate the number density of protein molecules at the interface using the molecular area provided by isotherms (A_m) and the fitted layer thickness (t_f) provided by the

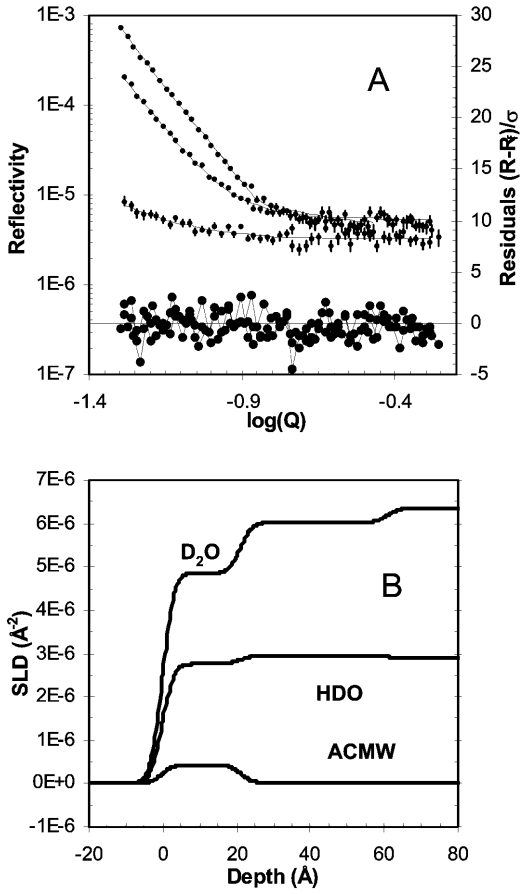

FIGURE 3 An example of three simultaneously fitted neutron reflectivity data sets, including error bars, fit, and residuals corresponding to bovine SP-B on saline buffer (salinity and pH vary somewhat in the three data sets; see text, 22°C) at 15 mN m^{-1} is shown in *A*. The corresponding fitted profile, which consists of two layers fitted as described in the text, is shown in *B*. In both panels the lower, middle, and upper fits correspond to subphases ACMW, HDO, and D_2O, respectively.

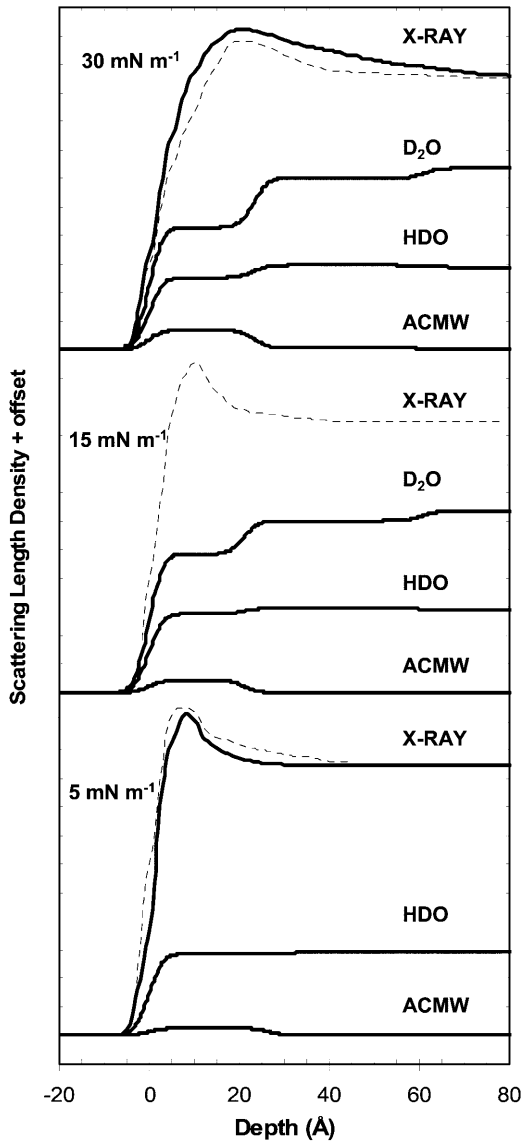

FIGURE 4 Models used to fit the available x-ray and neutron data. The three sets of models (bottom to top) correspond to pressures 5 mNm^{-1}, 15 mNm^{-1}, and 30 mNm^{-1}. Within each set the models (bottom to top) correspond to ACMW, HDO, and D_2O subphase (neutron reflectivity), and the corresponding x-ray measurement. Solid lines correspond to SP-B from cows, dashed lines (x-ray only) are of sheep SP-B. Ticks on vertical axis correspond to 1×10^{-6} Å^{-2}.

simultaneously fitted neutron models (for simplicity we only consider the layer at the air interface). This leaves us in a position to evaluate every term in the following expression for the scattering-length density (S) except n_w, the number of molecules of included water per protein molecule:

$$S = \frac{1}{A_m t_f}\left[\left(\sum_i b_i\right)_{\text{non-exch}} + \left(\sum_i b_i\right)_{\text{exch}} + \left(\sum_i b_i\right)_{\text{water}}\right]. \quad (1)$$

$$= \frac{1}{A_m t_f}\left[\left(\sum_i b_i\right)_{\text{non-exch}} + n_l\{\chi_D b_D + (1-\chi_D) b_H\} + n_w\left\{\chi_D\left(\sum_i b_i\right)_{D_2O} + (1-\chi_D)\left(\sum_i b_i\right)_{H_2O}\right\}\right]. \quad (2)$$

The three summed terms within the square brackets account for the nonexchanging atoms in the protein, the labile hydrogen atoms it contains, and included water, respectively. The solution for n_w follows:

$$n_w = \frac{SA_m t_f - \left(\sum_i b_i\right)_{\text{non-exch}} - n_l(\chi_D b_D + (1-\chi_D) b_H)}{\chi_D\left(\sum_i b_i\right)_{D_2O} + (1-\chi_D)\left(\sum_i b_i\right)_{H_2O}}. \quad (3)$$

This expression is ill conditioned (zero in the denominator) when the subphase is ACMW. This makes sense in that included ACMW will not contribute to the scattering caused by other components in the layer, so its quantity cannot be determined. For the HDO and D_2O subphases, substitution

TABLE 1 Parameters fitted in neutron models of Fig. 4

Pressure (mN m^{-1})	Upper thickness (Å)	Upper layer S ($\times 10^{-6}$ Å^{-2}) on subphase:			Lower thickness (Å)	Lower layer S ($\times 10^{-6}$ Å^{-2}) on subphase:		
		ACMW	HDO	D_2O		ACMW	HDO	D_2O
5	27(7)	0.25(5)	2.86(2)	–	–	–	–	–
15	21.2(9)	0.43(3)	2.76(2)	4.85(11)	39.7(12)	0.01(3)	2.949(13)	6.0(2)
30	23.4(7)	0.69(2)	2.53(3)	4.29(10)	37.9(19)	0.07(2)	2.962(13)	6.02(2)

Values in parentheses are the standard errors assuming negligible covariance. The background scatter was also fitted in each case.

of the fitted scattering-length densities into this expression gives the results shown in Table 2, which are in pleasing mutual agreement.

It is of interest to know what fraction (F_w) of the layer's volume can be attributed to the included water. To calculate this, we need an estimate of the mass of the protein divided by the volume it occupies, its ''water-free density,'' ρ_{prot}. This can be conveniently estimated by analogy with a chemically similar substance, such as the polyamide nylon, density $\sim$1.2 g cm^{-3}. Molecular volume arguments permit the following expression for F_w:

$$F_w = \frac{n_w M_{H_2O}/\rho_{H_2O}}{n_w M_{H_2O}/\rho_{H_2O} + M_{prot}/\rho_{prot}}. \quad (4)$$

For layers on ACMW we can reconcile the fitted SLD (S_f) and calculated SLD (S_c) using the relation $S_f = F_p \times S_c$, in which the proportionality factor F_p is the fractional volume of the layer occupied by the protein. Here S_c is calculated using the molecular mass of the partially deuteron-exchanged protein in isolation, with nylon again providing the water-free density estimate. It follows that:

$$F_w = 1 - F_p = 1 - S_f/S_c. \quad (5)$$

Values of F_w calculated by these approaches are listed in Table 2.

Table 2 shows a clear reduction in the amount of included water as the film is compressed, as one might expect. On the other hand, the fractional volume occupied by the water appears rather high for such a hydrophobic protein, suggesting that it does not pack neatly at the interface. This is likely due in large measure to mutual repulsion caused by the strong positive charge of the protein (+10 per dimer at pH 7), a notion supported by the work of Holt (Holt et al., 2000), Su (Su et al., 1998, 1999) and Lu (Lu et al., 1999) who investigated the pH dependence of the density.

TABLE 2 The number (n_w) of water molecules and their fractional volume (F_w) included in the SP-B monolayer at 5 mN m^{-1}, 15 mN m^{-1}, and 30 mN m^{-1}

Pressure (mN m^{-1})	A_m (Å^2)	t_m (Å)	n_w		F_w		
			HDO	D_2O	ACMW	HDO	D_2O
5	2700	27	1847	–	0.83	0.70	–
15	2200	21.2	933	864	0.71	0.54	0.52
30	1400	23.4	409	417	0.54	0.34	0.34

DISCUSSION

Structure of bovine SP-B

The peptide sequence of bovine SP-B was determined by Olafson (Olafson et al., 1987) in 1987. Based on that sequence, it has been proposed (Haagsman and Diemel, 2001; Johansson et al., 1991) that the structure of SP-B might be unusual in cows, owing to the relatively small proportion of cysteine in comparison with SP-B from other species. We note that the original assignment of several bovine residues was tentative, in particular residues 46 (an otherwise conserved cysteine linked to Cys-35) and 48 (the cysteine invoked in homodimer formation). It has been reported that the Cys-35/Cys-46 disulfide bond is critical for intracellular trafficking of SP-B (Beck et al., 2000), whereas our own and other (Nag et al., 1999) mass spectral results indicate that bovine SP-B is dimeric through disulfide bonds (Yu et al., 1987). The similarity of our results for bovine and ovine SP-B is consistent with the proposition that the protein sequences and structures are largely conserved.

Structural model

To date there is little direct evidence for the tertiary or quaternary structure of native SP-B, but the available data points to the structure described by Zaltash (Zaltash et al., 2000). This model is based on structural similarities to NK-lysin (Andersson et al., 1995), a protein for which a solution-phase NMR structure has been obtained (Liepinsh et al., 1997). The N- and C-terminal helices (helices 1 and 5, respectively) in each monomer are locked in an antiparallel arrangement by a pair of disulfide bonds, whereas helices 2 and 3 are kept in an antiparallel hairpin arrangement by another internal disulfide bond. Interestingly, the tertiary structure proposed by Zaltash does not present an obviously hydrophobic face to its external environment; because the five helices wrap onto each other in such a way that the hydrophobic stretches on the amphipathic helices are all in mutual contact.

Physical models suggest that this tertiary structure can be unfolded into a flat structure which for each monomeric half looks approximately like a boomerang, with helices 1 and 2 (at the N-terminus) forming the concave edges and helices 3, 4, and 5 forming the convex edges (see Fig. 5). One face of this unfolded structure is almost entirely hydrophobic,

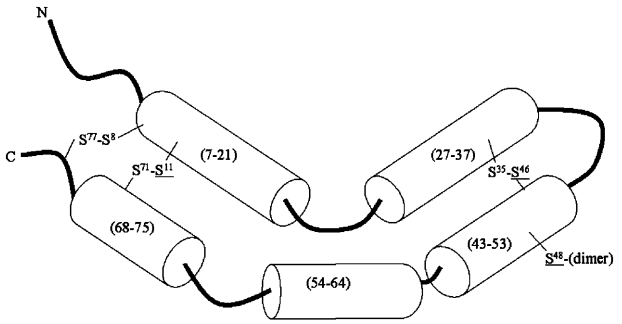

FIGURE 5 We propose that SP-B's tertiary structure can lay flat when by itself at an air-water interface. With the helices constrained as shown by the intramolecular disulfides, this view would presents the hydrophobic face of each alpha helix to the viewer. Numbers in the figure correspond to amino acid residues.

whereas the other face is largely hydrophilic, and it is clear how such an amphiphilic structure would orient at an air-water interface. Such unfolding would approximately double the area presented by the protein at the air-water interface.

Interestingly, the homodimer is held together by both a disulfide bond and a conserved acid-base pair (Zaltash et al., 2000) in such a way that the protein is unable to present the hydrophilic faces of both monomeric halves to the subphase at the same time. It is possible that the acid-base pair breaks when the protein is spread at the interface in order to enable this. There are only two acidic residues in the largely basic SP-B, and both are conserved, though the location of one of them varies from residue 59–63. Perhaps the latter acidic residue has a role to play in the flattened version of SP-B, or in interactions with the zwitterionic DPPC.

Isotherms

There have been relatively few studies of native SP-B at the air-water interface. A strong indication that the α-helices lie flat at the interface at low pressure comes from the limiting areas of Dieudonne's isotherms of peptides SP-B_{1-20} and SP-B_{9-36}, both of which involve amphipathic α-helices (Dieudonne et al., 2001). Extrapolating those results ($\sim$0.21 nm^2 $residue^{-1}$) to the 158 residues in the native dimeric protein suggests that it would occupy $\sim$33 nm^2 per dimer if the helices were all laid flat at the interface as in Fig. 5. For their globular NK-lysin-based SP-B dimer model, Zaltash (Zaltash et al., 2000) describes ''approximate (linear) dimensions of 55 $\times$ 37 Å,'' pointing to a close-packed molecular area in the vicinity of $\sim$15 nm^2 per dimer. We therefore propose that the $\sim$15$\rightarrow$40 nm^2 $dimer^{-1}$ region of the isotherms in Fig. 1 (in which our protein concentration was scaled to match Taneva's (Taneva and Keough, 1994) porcine SP-B isotherm) represents the reversible pressure-induced folding of the protein.

In the $\sim$15$\rightarrow$40 nm^2 $dimer^{-1}$ region the SP-B isotherms are linear with a shallow slope ($\sim$0.5 mN m^{-1} per 1% change in molecular area). By way of a familiar comparison, DPPC isotherms are very steep in the condensed-phase region as a result of close packing of the hydrocarbon chains ($\sim$2.6 mN m^{-1} per 1% change in molecular area, data not shown). The comparison suggests that the folding of SP-B into its high-pressure conformation is a gradual process as the pressure increases. The integral under the isotherm represents the system's energy change in going from molecules spread out at the interface to balled-up molecules. From the baseline to the point of collapse the isotherm is fairly linear, allowing us to estimate this integral as 4 $\times$ 10^{-19} J $molecule^{-1}$ or 260 kJ mol^{-1}.

There is considerable hysteresis associated with the collapse at $\sim$36 mN m^{-1} from which it is clear that the moderate rate of compression used (20 cm^2 min^{-1} on a 300 cm^2 trough) was rather too fast for the kinetics of the system. That this hysteresis is largely due to structural changes associated with the collapse is clear from the relative lack of hysteresis in the final short cycle presented in Fig. 1, in which the collapse area was not attained.

Support for this model from x-ray reflectivity

The fitted SLD profiles in Fig. 4 show fairly clearly that at surface pressures below $\sim$20 mN m^{-1} the most electron-dense part of the protein monolayer is within $\sim$10 Å of the air interface. Such SLD profiles are remarkably similar to those observed by Holt (Holt et al., 2000) for myoglobin at interfaces, who proposed changes in the tertiary structure of that protein such that its amphipathic α-helices were laid flat. In our model illustrated in Fig. 5, this region will correspond to the location of electron-dense regions of the protein monolayer, in particular the protein's relatively electron-rich disulfide linkages.

At pressures above 20 mN m^{-1} but below the collapse at $\sim$36 mN m^{-1}, the SLD profiles show a much shallower electron density gradient from the air toward the maximum, which now lies $\sim$20 Å from the air interface. At such pressures we believe that the protein is essentially in the globular conformation proposed by Zaltash, with both halves of the dimer at the interface. There is an orientation of the dumbbell-shaped dimer which would position almost all the sulfur in the protein at such a considerable depth from the surface; this has the dimer's C_2 axis coincident with the surface normal, with helix 3 of each monomer almost parallel to it. It is harder to determine whether the N-termini of helices 3 would be up or down, since the sulfur atoms are located fairly centrally within the folded protein. However, we tentatively propose that the N-termini of helices 3 are uppermost on the grounds that it is easier to see how the protein would end up in this orientation at the conclusion of the process of folding from the flat structure (Fig. 5). One can be confident that recent advances in reflectivity fitting based on molecular modeling (Politsch, 2001) will greatly assist such interpretations in the future.

One must be extremely wary of over interpreting the SLD profile in cases where the contrast with the subphase becomes very poor. Unfortunately, this renders the true thickness of the protein layer somewhat speculative because the hydrophilic parts of the protein, which can be expected to be at the interface of the protein with the subphase, will contain an increasing proportion of included solvent as well as a relatively high proportion of exchangeable protons. Consequently we do not expect the boundary to be distinct from the standpoint of reflectivity.

CONCLUSIONS

An algorithm for fitting arbitrary scattering-length density profiles at the available resolution of a given reflectivity profile has been developed and applied to monolayers of the crucial pulmonary surfactant protein, SP-B. In conjunction with pressure-area isotherms and existing models of the protein, the resulting x-ray SLD profiles suggest that SP-B unfolds at low surface pressure when placed by itself at an air-water interface with its amphipathic alpha helices lying largely in the plane of the interface. As the molecules at such an interface are squeezed together, the protein folds up and may assume the globular dumbbell shape proposed by Zaltash (Zaltash et al., 2000), and we are able to tentatively assign an orientation for the protein in this state. At molecular areas less than $\sim$15 nm^2 molecule^{-1}, the monolayer visibly collapses, but remains associated with the interface. The neutron-reflectivity results indicate the exchange of the protein's labile protons as well as a very substantial amount of included water in the protein monolayers.

We draw attention to the fact that the model proposed here takes no account of the protein's interaction with lipids (a topic of primary importance in natural lung surfactant which will be addressed in a subsequent publication). Instead, it serves to suggest the conformational flexibility of the protein in a way that we trust will lead to models for its interaction with lipids. We propose that such conformational changes are crucial to the functionality of SP-B since they point to a mechanism by which cycling of other surfactant components could occur, involving the reversible pressure-induced interment of amphipathic helices in the subphase. This work will also be of interest in the study of other amphipathic proteins (Weinberg et al., 2000).

Many faces have been associated with this work at some stage, especially in the early days of the project, and for this we would particularly like to thank Ms. Kylie Dean, Ms. Parimala Vajjhala, and Mr. Chris Wood. We are indebted to Mr. Ben O'Driscoll and Dr. Jian-Bang Peng for contributing their time to assist manning of the overseas facilities. We express our gratitude to Jan Johansson for making his NK-lysin-based SP-B model (Zaltash et al., 2000) available to us.

This work was enabled by an Australian Synchrotron Research Program Fellowship awarded to W.K.F, and access to synchrotron and neutron scattering facilities was possible thanks to funding provided by the Australian Access to Major Facilities program.

REFERENCES

Andersson, M., T. Curstedt, H. Jornvall, and J. Johansson. 1995. An amphipathic helical motif common to tumourolytic polypeptide NK-lysin and pulmonary surfactant polypeptide SP-B. *FEBS Lett.* 362:328–332.

Beck, D. C., C.-L. Na, J. A. Whitsett, and T. E. Weaver. 2000. Ablation of a critical surfactant protein B intramolecular disulfide bond in transgenic mice. *J. Biol. Chem.* 275:3371–3376.

Bligh, E. G., and W. J. Dyer. 1959. A rapid method of total lipid extraction and purification. *Canadian Journal of Biochemistry and Physiology.* 37:911–917.

Braslau, A., P. S. Pershan, G. Swislow, B. M. Ocko, and J. Als-Nielsen. 1988. Capillary waves on the surface of simple liquids measured by x-ray reflectivity. *Phys. Rev. A.* 38:2457–2470.

Brown, A. S., S. A. Holt, P. M. Saville, and J. W. White. 1997. Neutron and x-ray reflectometry: solid multilayers and crumpling films. *Australian Journal of Physics.* 50:391–405.

Bunger, H., R. P. Kruger, S. Pietschmann, N. Wustneck, L. Kaufner, R. Tschiersch, and U. Pison. 2001. Two hydrophobic protein fractions of ovine pulmonary surfactant: isolation, characterization, and biophysical activity. *Protein Expr. Purif.* 23:319–327.

Casals, C. 2001. Role of surfactant protein A (SP-A)/lipid interactions for SP-A functions in the lung. *Pediatr. Pathol. Mol. Med.* 20:249–268.

Cruz, A., C. Casals, and J. Perez-Gil. 1995. Conformational flexibility of pulmonary surfactant proteins SP-B and SP-C, studied in aqueous organic solvents. *Biochim. Biophys. Acta.* 1255:68–76.

Curstedt, T., H. Jornvall, B. Robertson, T. Bergman, and P. Berggren. 1987. Two hydrophobic low-molecular-mass protein-fractions of pulmonary surfactant – characterization and biophysical activity. *Eur. J. Biochem.* 168:255–262.

Daillant, J., J. J. Benattar, and L. Bosio. 1990. X-ray reflectivity study of monolayers of amphiphilics at the air-water-interface. *J. Phys. Condens. Matter.* 2:SA405–SA410.

Dieudonne, D., R. Mendelsohn, R. S. Farid, and C. R. Flach. 2001. Secondary structure in lung surfactant SP-B peptides: IR and CD studies of bulk and monolayer phases. *Biochim. Biophys. Acta.* 1511:99–112.

Haagsman, H. P., and R. V. Diemel. 2001. Surfactant-associated proteins: functions and structural variation. *Comp. Biochem. Physiol. A Mol. Integr. Physiol.* 129:91–108.

Helm, C. A., P. Tippmannkrayer, H. Mohwald, J. Alsnielsen, and K. Kjaer. 1991. Phases of phosphatidyl ethanolamine monolayers studied by synchrotron x-ray-scattering. *Biophys. J.* 60:1457–1476.

Holt, S. A., D. J. McGillivray, S. Poon, and J. W. White. 2000. Protein deformation and surfactancy at an interface. *J. Phys. Chem. B.* 104:7431–7438.

Johansson, J., T. Curstedt, and H. Jornvall. 1991. Surfactant protein B: disulfide bridges, structural properties, and kringle similarities. *Biochemistry.* 30:6917–6921.

Krol, S., M. Ross, M. Sieber, S. Kunneke, H.-J. Galla, and A. Janshoff. 2000. Formation of three-dimensional protein-lipid aggregates in monolayer films induced by surfactant protein B. *Biophys. J.* 79:904–918.

Liepinsh, E., M. Andersson, J. M. Ruysschaert, and G. Otting. 1997. Saposin fold revealed by the NMR structure of NK-lysin. *Nat. Struct. Biol.* 4:793–795.

Lu, J. R., T. J. Su, and R. K. Thomas. 1999. Structural conformation of bovine serum albumin layers at the air-water interface studied by neutron reflection. *J. Colloid Interface Sci.* 213:426–437.

Nag, K., J. G. Munro, K. Inchley, S. Schurch, N. O. Petersen, and F. Possmayer. 1999. SP-B refining of pulmonary surfactant phospholipid films. *Am. J. Physiol.* 277:L1179–L1189.

Olafson, R. W., U. Rink, S. Kielland, S. H. Yu, J. Chung, P. G. Harding, and F. Possmayer. 1987. Protein sequence analysis studies on the low molecular weight hydrophobic proteins associated with bovine pulmonary surfactant. *Biochem. Biophys. Res. Commun.* 148:1406–1411.

Oosterlaken-Dijksterhuis, M. A., H. P. Haagsman, L. M. G. Vangolde, and R. A. Demel. 1991. Characterization of lipid insertion into

monomolecular layers mediated by lung surfactant proteins SP-B and SP-C. *Biochemistry*. 30:10965–10971.

Oviedo, J. M., C. Casals, and J. Perez-Gil. 2001. Pulmonary surfactant protein SP-B is significantly more immunoreactive in anionic than in zwitterionic bilayers. *FEBS Lett*. 494:236–240.

Pastrana-Rios, B., S. Taneva, K. M. W. Keough, A. J. Mautone, and R. Mendelsohn. 1995. External reflection absorption infrared spectroscopy study of lung surfactant proteins SP-B and SP-C in phospholipid monolayers at the air/water interface. *Biophys. J*. 69:2531–2540.

Penfold, J., and R. K. Thomas. 1990. The application of the specular reflection of neutrons to the study of surfaces and interfaces. *J. Phys. Condens. Matter*. 2:1369–1412.

Penfold, J., R. C. Ward, and W. G. Williams. 1987. A time-of-flight neutron reflectometer for surface and interfacial studies. *J. Phys. [E]*. 20:1411–1417.

Pérez-Gil, J., A. Cruz, and C. Casals. 1993. Solubility of hydrophobic surfactant proteins in organic solvent/water mixtures. Structural studies on SP-B and SP-C in aqueous organic solvents and lipids. *Biochim. Biophys. Acta*. 1168:261–270.

Politsch, E. 2001. String Fit: a new structurally oriented x-ray and neutron reflectivity evaluation technique. *J. Appl. Crystallogr*. 34:239–251.

Review Issue of *Biochimica et Biophysica Acta*. 1998. Molecular basis of disease. *Biochim. Biophys. Acta*. 1408:77–361.

Review Issue of *Comparative Biochemistry and Physiology*. 2001. Part A: molecular & integrative physiology. *Comp. Biochem. Physiol*. 129:1–303.

Review Issue of *Pediatric Pathology and Molecular Medicine*. 2001. *Pediatr. Pathol. Mol. Med*. 21:249–536.

Schalke, M., P. Kruger, M. Weygand, and M. Losche. 2000. Submolecular organization of DMPA in surface monolayers: beyond the two-layer model. *Biochim. Biophys. Acta*. 1464:113–126.

Schalke, M., and M. Losche. 2000. Structural models of lipid surface monolayers from x-ray and neutron reflectivity measurements. *Adv. Colloid Interface Sci*. 88:243–274.

Schlossman, M. L., D. Synal, Y. M. Guan, M. Meron, G. Shea-McCarthy, Z. Q. Huang, A. Acero, S. M. Williams, S. A. Rice, and P. J. Viccaro. 1997. A synchrotron x-ray liquid surface spectrometer. *Rev. Sci. Instrum*. 68:4372–4384.

Su, T. J., J. R. Lu, R. K. Thomas, and Z. F. Cui. 1999. Effect of pH on the adsorption of bovine serum albumin at the silica water interface studied by neutron reflection. *J. Phys. Chem. B*. 103:3727–3736.

Su, T. J., J. R. Lu, R. K. Thomas, Z. F. Cui, and J. Penfold. 1998. The conformational structure of bovine serum albumin layers adsorbed at the silica-water interface. *J. Phys. Chem. B*. 102:8100–8108.

Takamoto, D. Y., M. M. Lipp, A. von Nahmen, K. Y. C. Lee, A. J. Waring, and J. A. Zasadzinski. 2001. Interaction of lung surfactant proteins with anionic phospholipids. *Biophys. J*. 81:153–169.

Taneva, S., and K. M. W. Keough. 1994. Pulmonary surfactant proteins SP-B and SP-C in spread monolayers at the air-water-interface.1. Monolayers of pulmonary surfactant protein SP-B and phospholipids. *Biophys. J*. 66:1137–1148.

Taneva, S. G., J. Stewart, L. Taylor, and K. M. W. Keough. 1998. Method of purification affects some interfacial properties of pulmonary surfactant proteins B and C and their mixtures with dipalmitoylphosphatidylcholine. *Biochim. Biophys. Acta*. 1370:138–150.

Weaver, T. E., and J. J. Conkright. 2001. Function of surfactant proteins B and C. *Annu. Rev. Physiol*. 63:555–578.

Weinberg, R. B., V. R. Cook, J. A. DeLozier, and G. S. Shelness. 2000. Dynamic interfacial properties of human apolipoproteins A-IV and B-17 at the air/water and oil/water interface. *J. Lipid Res*. 41:1419–1427.

Yu, S. H., W. Chung, R. W. Olafson, P. G. Harding, and F. Possmayer. 1987. Characterization of the small hydrophobic proteins associated with pulmonary surfactant. *Biochim. Biophys. Acta*. 921:437–448.

Zaltash, S., M. Palmblad, T. Curstedt, J. Johansson, and B. Persson. 2000. Pulmonary surfactant protein B: a structural model and a functional analogue. *Biochim. Biophys. Acta*. 1466:179–186.